PHYSICAL REVIEW B VOLUME 31, NUMBER 10 15 MAY 1985

Characterization of intermixing at metal-semiconductor interfaces by angle-resolved Auger-electron emission: Cu/Si(111)-7×7

S. A. Chambers and G. A. Howell
Department of Chemistry, Bethel College, St. Paul, Minnesota 55112

T. R. Greenlee
Department of Physics, Bethel College, St. Paul, Minnesota 55112

J. H. Weaver
Department of Chemical Engineering and Materials Science, University of Minnesota, Minneapolis, Minnesota 55455
(Received 4 October 1984; revised manuscript received 26 December 1984)

Si($L_{2,3}VV$) and Cu($M_{2,3}VV$) Auger intensities from the Cu/Si(111)-7×7 interface have been measured in a polar-angle-resolved fashion for various Cu thicknesses. A simple theory of polar-angle-resolved Auger emission has been developed and used to extract atom-number densities for both Si and Cu as a function of depth. It is found that significant Si outdiffusion is triggered at 300 K by Cu coverage in excess of 2 Å with characteristic diffusion lengths for Si of ~35% of the overlayer thickness. Cu diffusion into the substrate, if it occurs at all, is limited to characteristic penetration depths of 1 to 2 Å for all coverages. The increased extent of Si outdiffusion above 2 Å is accompanied by substantial changes in Cu distribution throughout the interfacial region; at 2 Å, the Cu density increases sharply from interface boundary to surface whereas above 2 Å, the Cu density is constant throughout the interface.

I. INTRODUCTION

Condensation of metal atoms on single-crystal semiconductor surfaces leads to a wide variety of interesting physical and chemical phenomena.[1] Ordered layer-by-layer growth, cluster formation,[2] interdiffusion,[3,4] and chemical reaction[5] have been observed for different systems. Successful observation of these phenomena requires a wide repertoire of experimental probes; no one technique can provide all the necessary information to unambiguously model the microscopic development of the interface.

In this paper we address the issue of interdiffusion at a metal-semiconductor interface. This research was undertaken because knowledge of the atomic densities of the substrate and adsorbed material as a function of depth in the interface region is critical for characterizing interface properties. Most attempts to obtain such information have utilized argon-ion sputter profiling.[6–11] As discussed by some of these authors,[6–8] ion-induced surface damage, preferential sputter rates, implantation of sputtered species, depth calibration problems, and poor depth resolution render the quantitative reliability of this technique dubious, particularly when applied to ultrathin overlayers (a few angstroms). In order to overcome these difficulties, attempts have been made to obtain a better understanding of the sputtering process[9,11] and to quantitatively account for the phenomenon of sputter broadening.[9]

A nondestructive alternative to sputter profiling which eliminates many of the above problems utilizes the polar-angle dependence of Auger and photoelectrons emitted from both the substrate and overlayer. As originally demonstrated by Fadley and Bergstrom,[12] varying the collection angle relative to the plane of the surface leads to selective enhancement of bulk and surface signals. Most such studies to date have utilized core-level photoelectrons excited by either conventional x-ray sources[13] or synchrotron radiation.[14] One disadvantage of polar-angle resolved photoemission is that of data acquisition time. In order to obtain a complete polar intensity profile, a large number of spectra must be taken over the collection angle range 0° to 90°. A minimum of nine or ten spectra would allow a rough polar profile to be constructed, but 20 to 40 spectra would be desirable. Active metal overlayers will contaminate in the several-hour time span required to acquire such detailed data by means of photoemission.

A closely related yet much faster approach to the problem involves utilizing the polar-angle dependence of low-energy core-valence-valence (CVV) Auger-electron intensity. An excellent spectrum can be obtained in the pulse-counting $N(E)$ mode in just a few minutes. Moreover, low incident beam currents (a fraction of a microampere) can be used to minimize surface damage, and one still obtains very high count rates. In this article we describe the first use of polar-angle-resolved Auger emission to quantitatively study interdiffusion phenomena at a metal-semiconductor interface. The Cu/Si(111)-7×7 system was chosen because interdiffusion of Si into the overlayer has been observed and qualitatively studied with other surface analysis techniques,[3,4] including x-ray photoemission spectroscopy (XPS), ultraviolet photoemission spectroscopy (UPS), Auger-electron spectroscopy (AES), and low-energy electron diffraction (LEED).

This article is organized as follows: Section II describes the theory of polar-angle-resolved Auger emission as

developed for this particular application, Sec. III provides experimental details, Sec. IV presents experimental and theoretical results, Sec. V consists of a discussion of the work, and conclusions are drawn in Sec. VI.

II. THEORY OF POLAR-ANGLE-RESOLVED AUGER EMISSION FROM INTERMIXED OVERLAYERS

After an Auger electron has been rejected from an atom in a solid, it can be (1) inelastically scattered, leading to signal attenuation, (2) elastically scattered, leading to diffraction effects if the sample is a single crystal, and (3) refracted at the surface-vacuum interface. In this model we treat the overlayer as a uniform slab with a constant attenuation coefficient and ignore any single-crystal effects.

Figure 1 shows the relevant geometry of our sample-analyzer arrangement. Auger electrons originating a perpendicular distance y from the surface propagate with internal angle θ' to refract at the surface and travel toward the analyzer aperture with external angle θ. The principal factor which governs intensity variations with depth is inelastic attenuation. Thus, the intensity at a given depth y will be proportional to $\exp(-y/\Lambda\sin\theta')$, where Λ is the electron mean free path. In addition, surface refraction will bring about changes in intensity due to internal reflection and what is effectively an increase in Auger-electron flux caused by a reduction in the cross sectional area of the Auger-electron beam upon refraction. These effects add factors of $1-R$ and $\sin\theta'/\sin\theta$, respectively, where R is a reflection coefficient for Auger electrons within the sample incident on the surface.[15] Additional factors governing the observed intensity are incident electron-beam flux (I_0), Auger cross section (σ), sample area irradiated ($A/\sin\alpha$), solid angle of acceptance (Ω), detector efficiency (D), and emitting atom number density at depth y [$\rho(y)$]. Combining these factors, the differential intensity brought about by a volume element a perpendicular distance y from the surface is given by

$$dI(\theta,y)=\left[\frac{I_0\sigma A\Omega D}{\sin^2\alpha}\right]\left[(1-R)\frac{\sin\theta'}{\sin\theta}\right]\rho(y) \times\exp(-y/\Lambda\sin\theta')dy \ . \quad (1)$$

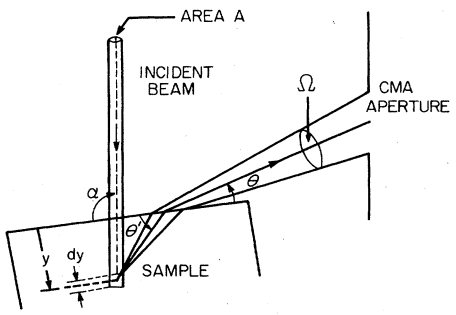

FIG. 1. Orientation of the sample with respect to the incident electron beam and analyzer aperture.

The propagation angle within the material (θ') is related to that outside by the conservation of $k_{||}$ rule which yields

$$\theta'=\cos^{-1}\left[\left[\frac{E_k-V_0}{E_k}\right]^{1/2}\cos\theta\right] . \quad (2)$$

E_k is the electron kinetic energy inside the material and V_0 is the inner potential. These refraction effects are very important at the kinetic energies of the CVV Auger transitions used here (~ 100 eV), particularly at low emission angles. As shown by Fadley,[15] the electron reflection coefficient can be estimated by treating the interaction of the electron with the surface as analogous to a particle penetrating a square well potential of height V_0, the inner potential of the material. From this model we get

$$R=\left[\frac{[1-(1-V_0/E_k\sin^2\theta')^{1/2}]}{[1+(1-V_0/E_k\sin^2\theta')^{1/2}]}\right]^2 . \quad (3)$$

With the exception of the cross section, the factors within the first set of large parentheses in Eq. (1) depend only on the spectrometer. The factors in the second set of large parentheses which account for the change in Auger-electron flux brought about by surface refraction, can be combined with the instrument factors and cross section to yield a function $F(\theta)$, defined as:

$$F(\theta)=\frac{I_0\sigma A\Omega D}{\sin^2\alpha}(1-R)\frac{\sin\theta'}{\sin\theta} . \quad (4)$$

This function accounts for everything except the emitting-atom number density in the material and electron attenuation, and should be essentially constant as coverage proceeds, provided the inner potential and cross section do not change substantially. Thus, if $F(\theta)$ is evaluated for each component in the interface, it could be used to deduce atomic densities in the intermixed phase. For single-crystals of Cu and Si, the inner potentials are 14 and 17 eV, respectively.[16,17] Therefore, we take 15 eV as an approximate value for the Cu-Si interface at all stages of development. In practice, we find that the calculated intensities are not particularly sensitive to the choice of V_0 over the range 14 to 17 eV. Changes in CVV Auger cross section for either Cu or Si would result from valence-band modification upon intermixing and are revealed by line-shape changes. No such changes have been observed for the Cu($M_{2,3}VV$) line. The Si($L_{2,3}VV$) line does split and broaden at higher Cu coverages due to p-d rehybridization, but the high degree of p character in the Si valence states both before and after intermixing with Cu suggests that this effect causes only a redistribution of Auger intensity over the multiplet.

For pure samples of either substrate or overlayer material, $\rho(y)$ is simply equal to ρ, the bulk atom number density for each material. In this case, Eq. (1) is easily integrated over y and $F(\theta)$ can be directly evaluated. The result is

$$F(\theta)=\frac{I(\theta)}{\rho\Lambda\sin\theta} . \quad (5)$$

Once determined for pure substrate (s) and overlayer (o) materials, $F_s(\theta)$ and $F_o(\theta)$ will be inserted into integrated

forms of Eq. (1) appropriate to the interface.

$I(\theta)$, and hence $F(\theta)$, as used in Eq. (5) represent an average over the 8° polar-angle resolution of our analyzer. For later use it is desirable to express $F(\theta)$ in units of per degree of polar angle. In order to make this adjustment, it is assumed that for all polar angles except 88°—90° and 0°—2°, $I(\theta)$ increases linearly with θ over all 8° polar-angle intervals. This approximation is reasonable in light of the observed behavior of $I(\theta)$ for both substrate and overlayer materials (to be discussed in more detail in Sec. IV). It then suffices simply to divide $I(\theta)$ by 8° for each value of θ prior to evaluating Eq. (5). The fact that $I(\theta)$ is observed to go through a maximum at $\theta=90°$ and go to 0 for $\theta<0°$ is used to perform a suitable adjustment to obtain an $I(\theta)$ per degree of polar angle for $\theta=88°$—90° and 0°—2°.

In order to extract concentration information from the interface polar profiles, a particular form of $\rho(y)$ for both substrate and overlayer material is assumed. Equation (1) can then be integrated to yield expressions for $I_s(\theta)$ and $I_o(\theta)$. For the substrate material,

$$I_s(\theta)=F_s(\theta)\int_0^\infty \rho_s(y)\exp(-y/\Lambda_s\sin\theta_s')dy \qquad (6)$$

and similarly for the overlayer. The function $\rho(y)$ contains one to three undetermined parameters which are chosen to generate the best fit with experiment. The fitting algorithm used is a combination of gradient search and linearization of the fitting function methods developed by Marquardt.[18] Further details on the exact choice of $\rho(y)$ are given in Sec. IV.

Finally, comparison of theoretical results with experimental polar profiles requires that the former, which come out per degree of polar angle, be integrated over the finite aperture size of 8°. This task is readily accomplished using Simpson's rule or the trapezoidal rule in the calculation of $I(\theta)$.

III. EXPERIMENTAL DETAILS

The system used to perform angle-resolved Auger spectroscopy is described in detail elsewhere.[19] The single-pass cylindrical mirror analyzer (CMA) with angle-resolving capability is also used as a LEED I-V detector, employing a modification first described by McDavid and Fain.[20] Single-crystal wafers of (111)-oriented p-type Si were cleaned by cycles of Ar-ion sputtering and heating to 800 °C. This procedure produced a clean 7×7 surface; no impurities were present as judged by Auger spectra taken at a surface-enhancing polar angle of 10°.

Evaporation of high-purity Cu was monitored by a quartz crystal oscillator. Pressures during evaporation never exceeded 2×10^{-10} torr and during polar scans were typically $7-9\times10^{-11}$ torr. Complete polar scans from normal emission to grazing emission were obtained by taking spectra every 2°. Replicate measurements at fixed angles indicated a standard deviation of 3—4% of the value of the mean. The total time required to complete a full polar scan was about 2 h, and grazing emission Auger spectra taken at the end of each run showed that the surface was free of contaminants. Polar profiles were obtained in the $(\bar{1}10)$ azimuthal plane perpendicular to the surface and in a plane rotated 30° from $(\bar{1}10)$. These were then averaged to remove as much diffraction modulation as possible, since our theoretical model ignores single-crystal effects. For future reference, we define the zero in ϕ as lying in the $(\bar{1}10)$ plane perpendicular to the surface.

4 keV electrons were used to excite the Auger transitions and incident beam currents were typically 0.1—0.5 μA. There was no evidence of electron-induced surface damage at any point, as judged by reproducible Auger intensities and LEED patterns over several hours of beam irradiation. Peak intensities were determined by smoothing the spectra, subtracting a linear background, and integrating. Spectra were then normalized to one another by dividing by the average number of background counts on the flat high-energy side of the Si($L_{2,3}VV$) peak, thus removing intensity variations brought about by drifts in the incident beam current.

IV. RESULTS

Figure 2 demonstrates how the Auger spectrum develops as a function of Cu coverage. Coverages are expressed in angstroms, and one angstrom of Cu equals 1.1 monolayer (ML) on the Si(111) surface. From 0—2 Å there is no significant change in the Si($L_{2,3}VV$) line shape. However, above 5 Å a triplet develops, indicating substantial modification of the valence states of Si as the normal sp^3 hybrid bonds are broken and Si diffuses into the Cu layer. Similar line shape changes have been observed as a function of coverage for Pt/Si(111),[21] Pd/Si(111),[22] and Cu/Si(111).[4] Using spectra taken at normal emission, one can construct a Si($L_{2,3}VV$) attenuation curve to determine the extent to which interdiffusion occurs.

Figure 3 shows a plot of $\ln[I(d)/I(0)]$ versus d, where d, $I(0)$, and $I(d)$ are the overlayer thickness, clean sur-

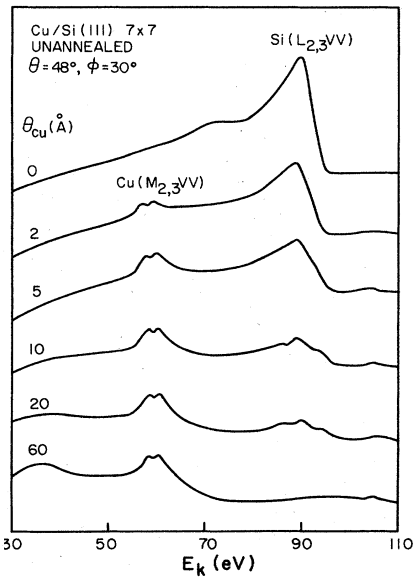

FIG. 2. Si($L_{2,3}VV$) and Cu($M_{2,3}VV$) Auger spectra as a function of Cu coverage in units of Å. 1 Å of Cu equals 1.1 monolayers on Si(111).

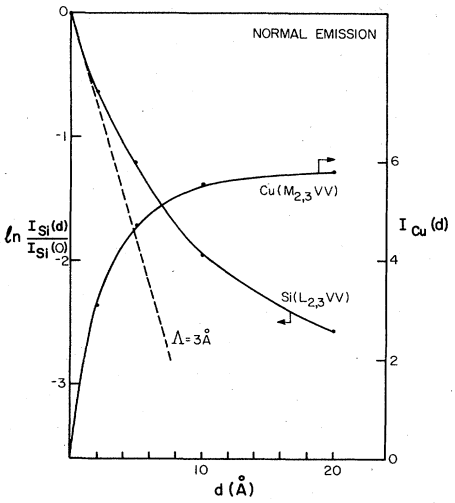

FIG. 3. Attenuation-growth curve for the unannealed Si-Cu interface. d is the overlayer thickness.

face Si($L_{2,3}VV$) intensity, and Si($L_{2,3}VV$) intensity with overlayer thickness d present, respectively. Each point is an average of four spectra taken at normal emission and the standard deviation of each data set is less than 4% of the mean for that set. Linear behavior with slope $-1/\Lambda$ is expected if the interface is sharp, and the observed positive deviation from linearity indicates outdiffusion of Si. The initial slope provides a good estimate of the mean free path for the Si($L_{2,3}VV$) electron moving through the overlayer. In this case, we get 2.8 ± 0.5 Å. In the evaluation of Eq. (5), we use a value of 3 Å. Also shown for reference is a growth curve for the Cu($M_{2,3}VV$) line.

Corresponding LEED data indicate relaxation of Si(111)-7×7 to a weakening Si(111)-1×1 pattern for 2 and 5 Å coverages, followed by the appearance at 10 Å of a Cu(111)-1×1 pattern rotated 30° with respect to the Si surface mesh. These results are in good agreement with those obtained by Ringeisen *et al.*[3]

In Figs. 4 and 5 we present polar-angle intensity profiles for the Si($L_{2,3}VV$) and Cu($M_{2,3}VV$) Auger intensities in two symmetry-inequivalent azimuthal planes. The top profiles in each panel correspond to pure Si (Fig. 4) or Cu (Fig. 5) and contain the information from which $F_s(\theta)$

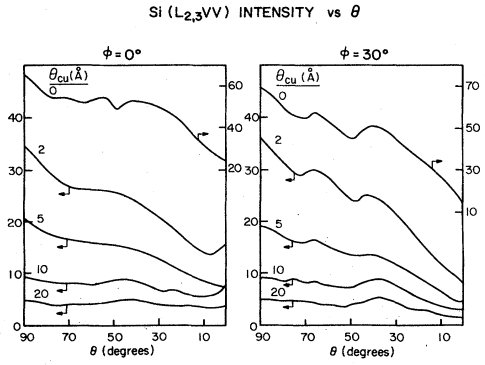

FIG. 4. Si($L_{2,3}VV$) polar intensity profile taken in two symmetry-inequivalent azimuthal planes perpendicular to the surface. No annealing.

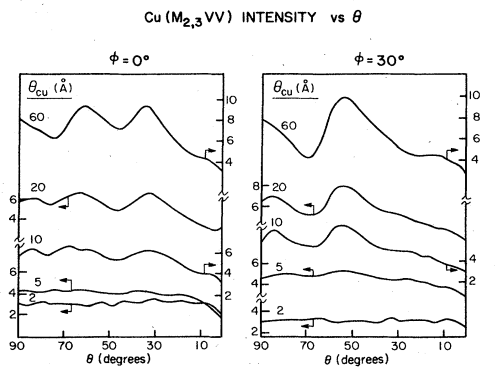

FIG. 5. Cu($M_{2,3}VV$) polar intensity profile taken in two symmetry-inequivalent azimuthal planes perpendicular to the surface. No annealing.

and $F_o(\theta)$ are evaluated [Eq. (5)]. At a coverage of 60 Å, no Si($L_{2,3}VV$) signal was present and the LEED I-V curves were those expected for a Cu(111) single-crystal surface film. Thus we take this surface as our reference surface for pure Cu(111).

The diffraction modulation observed in each case is a sensitive probe of the local structure of the emitting atom and can be used as a structural fingerprint at other coverages. At 2 Å coverage, the diffraction modulation observed for the clean Si(111)-7×7 surface is weakened but still present and the Cu profile is essentially featureless. Coupled with the weak Si(111)-1×1 LEED pattern and the attenuation curve in Fig. 3, these data suggest that the Cu layer grows in a weakly ordered layer-by-layer fashion, up to 2 Å. This mode of growth diminishes and gives rise to reaction and outdiffusion at 5 Å, as evidenced by the Si line-shape change and deviations from linearity of the Si($L_{2,3}VV$) attenuation curve (Fig. 3). By 10 Å, the Cu polar profiles show clear similarities to those of the 60 Å film [pure Cu(111)]. However, a significant amount of Si remains dispersed throughout the overlayer and the increased Si($L_{2,3}VV$) splitting indicates a more substantial chemical interaction with the Cu. There are no substantive changes between 10 and 20 Å, except that the overlayer is only slightly richer in Cu but poorer in Si by a factor of 2. At 60 Å, the evolution of the overlayer to a pure Cu(111) film is complete and no Si is present on the surface.

In the top panels of Figs. 6 and 7, we present average polar profiles for clean Si(111)-7×7 and a 60 Å Cu overlayer [essentially a pure Cu(111) surface]. Each profile is an average over two symmetry inequivalent azimuthal planes ($\phi=0°$ and $\phi=30°$). As can be seen, such averaging is not sufficient to remove all the diffraction features. Therefore, for the purpose of evaluating $F_s(\theta)$ and $F_o(\theta)$, we effectively smooth out the remaining diffraction modulation. Then, after adjusting the intensities for 8° angular resolution as discussed in Sec. II, these curves are used to evaluate $F(\theta)$ for Si($L_{2,3}VV$) and Cu($M_{2,3}VV$) Auger emission through the use of Eq. (5).

Also shown in Figs. 6 and 7 are the experimental polar profiles averaged over azimuthal planes at $\phi=0°$ and $\phi=30°$ compared to those predicted by Eq. (6) for the best

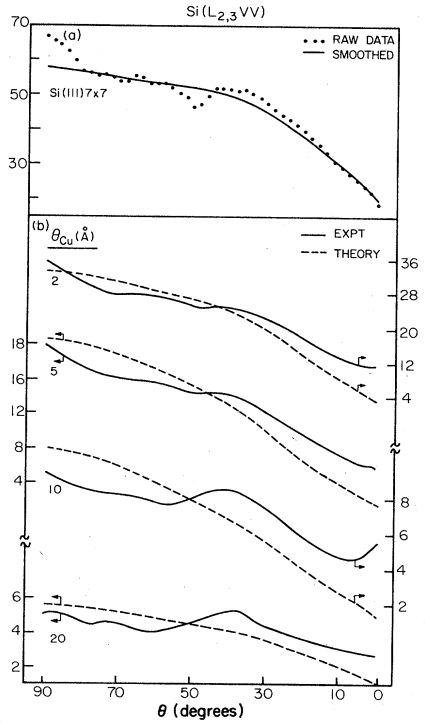

FIG. 6. (a) Clean surface Si($L_{2,3}VV$) polar profile averaged over two azimuthal planes, raw data, and smoothed to remove diffraction-induced fine structure. (b) Two-azimuth averaged experimental and calculated Si($L_{2,3}VV$) polar profiles using Eqs. 8(a) and 8(b) as a Si atom number density function.

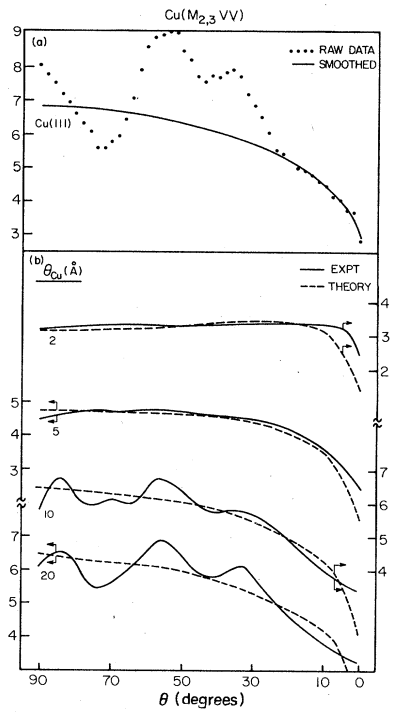

FIG. 7. (a) Cu($M_{2,3}VV$) polar profiles for a 60 Å Cu film [pure Cu(111)] averaged over two azimuthal planes, raw data, and smoothed to remove diffraction-induced fine structure. (b) Two-azimuth averaged experimental and calculated Cu($M_{2,3}VV$) polar profiles using Eqs. 10(a) and 10(b) for 2, 5, and 10 Å coverages and Eqs. 9(a) and 9(b) for the 20 Å coverage.

choice of density function. For both Si($L_{2,3}VV$) and Cu($M_{2,3}VV$) emission calculations, physically plausible atom number density functions of various forms with one, two, or three undetermined parameters were tried. For each function, the fitting routine determined the choice of parameters which yielded a minimum value of weighted χ^2. Turning first to the distribution of Si in the interface, a linear function and an exponential function were modeled. The linear function was of the form

$$\rho(y)=\begin{cases}\rho_0-a(d-y), & \text{for } y\le d \quad (7a)\\ \rho_0, & \text{for } y>d \quad (7b)\end{cases}$$

and the exponential function was of the form

$$\rho(y)=\begin{cases}\rho_0\exp[-a(d-y)], & \text{for } y\le d \quad (8a)\\ \rho_0, & \text{for } y>d. \quad (8b)\end{cases}$$

Here ρ_0 is the bulk atom number density of Si(5.018×10^{-2} atoms/Å^3), d is the overlayer thickness, a is the undetermined parameter, and y is the perpendicular distance measured from the surface. For all coverages, it is found that the exponential function gives a much better fit to the experimental data than does the linear function; χ^2 for the exponential function was 1.5 times lower at 2 Å coverage and 3 times lower at 20 Å coverage than the corresponding linear function values. For both functions, a mean free path of 3 Å was used, as discussed earlier. The quality of the fit is also reasonably sensitive to the choice of the undetermined parameter.

The sensitivity of the fit to both the choice of Si density function and undetermined parameter is illustrated in Fig. 8 for the 5 Å coverage. Here we plot experimental and theoretical Si($L_{2,3}VV$) polar profiles for (1) Eqs. (8a) and (8b) with various choices of undetermined parameter (a_{opt} and $a_{opt}\pm0.1$, where a_{opt} is the value of a which minimizes χ^2), and (2) Eqs. (7a) and (7b) with a optimized. The value of χ^2 resulting from use of the optimized form of Eqs. (7a) and (7b) is twice that which results from using optimized Eqs. (8a) and (8b). Furthermore, if a in Eqs. (8a) and (8b) is increased and decreased by 0.1 from its optimal value of 0.602, χ^2 increases by 40% and 75%, respectively. Therefore, it appears that a unique, physically reasonable Si density function which yields maximum agreement with experiment can be derived from these data. The best values of a and the predicted Si atom number densities on the surface are given in Table I.

From Table I, it is clear that the calculated surface Si density is an order of magnitude lower at 2 Å than that for the 5, 10, and 20 Å overlayers, indicating a substantial increase in outdiffusion above 2 Å. Moreover, for all coverages above 2 Å, the characteristic penetration depth (distance into the overlayer by which the Si density has decayed to $1/e$ of its bulk value) is approximately 35% of the overlayer thickness, whereas for 2 Å it is only about 20% of the overlayer thickness. These results are supported by the observed change in Si($L_{2,3}VV$) line

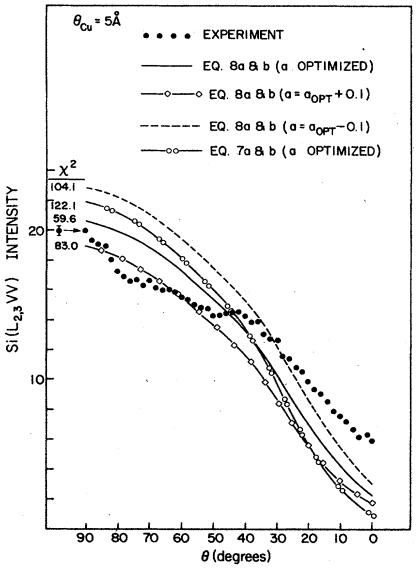

FIG. 8. Experimental and theoretical Si($L_{2,3}VV$) polar profiles for a 5 Å Cu coverage illustrating the sensitivity of the method to the choice of density function and undetermined parameter. The experimental error representative of a given Auger intensity is shown by the error bar. The values of unweighted χ^2 (defined as $\sum_{\theta=0^\circ}^{90^\circ,2^\circ}[I_{\text{calc}}(\theta)-I_{\text{expt}}(\theta)]^2/\sigma^2_{\text{expt}}$) are shown for each theoretical polar profile.

shape above 2 Å.

For the Cu distribution calculation, we have used a linear function which terminates discontinuously at the Cu-Si interface and a linear function with an exponential tail into the substrate. In analytical form, the functions are

$$\rho(y)=\begin{cases}\rho_s+a_1 y, & \text{for } y\le d \\ 0, & \text{for } y>d\end{cases} \tag{9a}$$

(9b)

and

$$\rho(y)=\begin{cases}\rho_s+a_1 y, & \text{for } y\le d \\ (\rho_s+a_1 d)\exp[-a_2(y-d)], & \text{for } y>d\end{cases} \tag{10a}$$

(10b)

Here, ρ_s is the Cu number density at the surface (a free parameter), d and y are as defined previously, and a_1 and a_2 are undetermined parameters. When necessary, the parameter a_1 was constrained to be 0 or negative, and less than or equal in magnitude to ρ_s/d, ensuring that the fitting program would not seek a solution in which the Cu density increases from surface to interface. This constraint is realistic in that the Si density *does* increase from surface to interface, and thus, the Cu density is expected to either decrease or remain constant. The parameter a_2 was free to vary. The Cu($M_{2,3}VV$) mean free path was determined by performing a two-parameter fit on the 20 Å coverage and employing a linear density function of the form $\rho(y)=0.078+a_1 y$, where a_1 and Λ were allowed to vary. The value 0.078 was chosen because values of 0.078 and 0.079 routinely result from two-parameter fits using the form $\rho(y)=\rho_s+a_1 y$ with a fixed value of Λ taken from the universal mean-free-path curve.[23] This calculation generates a value of 3.6 Å for Λ, which is used in all subsequent calculations. In general, the χ^2 values resulting from the use of Eqs. (9a), (9b), (10a), and (10b) are comparable for all coverages. This agreement is due to the rather small extent of Cu indiffusion predicted by Eqs. (10a) and (10b); characteristic diffusion lengths of only 1–2 Å result for the 2, 5, and 10 Å coverages. However, for a given choice of density function, the fit is quite sensitive to the choice of ρ_s, as illustrated in Fig. 9. Here we present for a 5 Å coverage, experimental and theoretical polar profiles using (1) Eqs. (9a), (9b), (10a), and (10b) with all parameters optimized, and (2) both functions with their respective values of ρ_s reduced from optimal numbers by 0.01 (a decrease of $\sim$14%). Such reductions in ρ_s cause χ^2 to be increased by factors of 12 and 15 for Eqs. (9a), (9b), (10a), and (10b), respectively. The high degree of sensitivity of the fit to ρ_s is not surprising in that a_2 converges to zero for both functions, rendering a constant

TABLE 1. Model predictions for surface silicon number densities. $\rho_{Si}(y)=\rho_0\exp[-a(d-y)]$.

d (Å)	a	Surface atom number density (atoms/ Å^3)
2	2.51	3.34×10^{-4}
5	0.602	2.47×10^{-3}
10	0.282	3.00×10^{-3}
20	0.143	2.85×10^{-3}

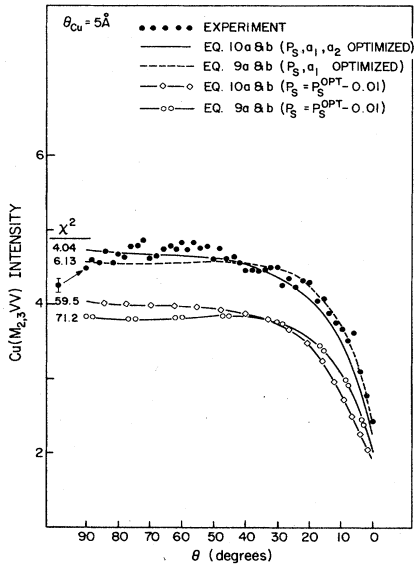

FIG. 9. Experimental and theoretical Cu($M_{2,3}VV$) polar profiles for a 5 Å Cu coverage illustrating the sensitivity of the method to the choice of density function and undetermined parameter. The experimental error representative of a given Auger intensity is shown by the error bar. The values of unweighted χ^2 (defined as $\sum_{\theta=0^\circ}^{90^\circ,2^\circ}[I_{\text{calc}}(\theta)-I_{\text{expt}}(\theta)]^2/\sigma^2_{\text{expt}}$) are shown for each theoretical polar profile.

Cu density of ρ_s in the interfacial region.

The goodness of the fit resulting from either Eqs. (9a) and (9b) or (10a) and (10b) makes the choice of Cu density function considerably less obvious than in the case of Si. However, the LEED results at low coverage provide a valuable clue. As mentioned in Sec. IV, a Si(111)-1×1 pattern persists for the first few monolayers of Cu, suggesting an epitaxial growth model. Thus we expect that the Cu density at the interface boundary should be close to the Si bulk density. In all cases, Eqs. (9a) and (9b) predict a Cu interface density which is considerably larger than that of bulk Si. Equations (10a) and (10b) also predict an interface Cu density which is larger than that of bulk Si for three of the four coverages, but less than that generated by Eqs. (9a) and (9b). Thus, we judge Eqs. (10a) and (10b) to be marginally preferable to Eqs. (9a) and (9b) in describing the Cu atom number density in the interfacial region for Cu deposits of 2, 5, and 10 Å. The resulting values of ρ_s, a_1, and a_2 are shown in Table II. For 2 Å, Eqs. (10a) and (10b) predict a sharp decrease in Cu density from 0.101 atoms/Å^3 at the surface to 0.0424 atoms/Å^3 at the interface. On the other hand, at 5 and 10 Å, the Cu density is predicted to be constant throughout the interface with values of 0.0687 and 0.0817 atoms/Å^3, respectively. For all these coverages, characteristic diffusion lengths for Cu are predicted to be only 1–2 Å.

95% of a given Auger signal originates within a depth of 3Λ [11 Å for the Cu($M_{2,3}VV$) electron]. Therefore, we have no sensitivity to the interface boundary when d is 20 Å. Thus, we use Eqs. (9a) and (9b) to calculate Cu densities in the top 10–11 Å of the overlayer. Here, we do not constrain a_1 and a slight Cu density increase is predicted from surface to interface boundary. Moreover, the Cu density converges to a value quite close to the bulk Cu value at the surface, in good agreement with the LEED results which showed the ordered Cu(111) pattern.

The overall results are best summarized by plotting the calculated Si and Cu atom number densities as a function of distance from the interface boundary, as shown in Fig. 10. One striking observation is that the Si surface density is an order of magnitude smaller and the Cu surface density is 20% to 30% larger at 2 Å than at higher coverages. This result indicates that Cu builds up on the surface prior to the strong Si-Cu interaction, the surface disruption, and the onset of Si outdiffusion. This interface therefore exhibits a reaction triggered by Cu coverage in excess of 2 Å but not at lower coverage. A second important observation is that for the 10 and 20 Å, the total atom number density within the first few angstroms of the interfacial region exceeds that of either pure Si or pure Cu but rapidly approaches the bulk Cu value with increasing distance from the interface boundary. This result suggests that the interface is an intermixed Cu-Si phase, with Cu being the predominant element and Si being dissolved in the matrix to a decreasing extent as the surface is approached.

TABLE II. Model predictions for Cu atom number densities. $\rho_{Cu}(y)=\rho_s+a_1 y$ for $y \le d$ at all coverages; $\rho_{Cu}(y)=0$ for $y>d$ and $d=20$ Å; $\rho_{Cu}(y)=(\rho_s+a_1 d)\exp[-a_2(y-d)]$ for $y>d$ and $d=2$, 5, and 10 Å. (ρ_s is the surface atom number density.)

d(Å)	ρ_s(atoms/ Å^3)	a_1 ($\times 10^2$)	a_2
2	0.101	−2.93	0.667
5	0.0687	0	0.452
10	0.0817	0	0.923
20	0.0793	0.0127	

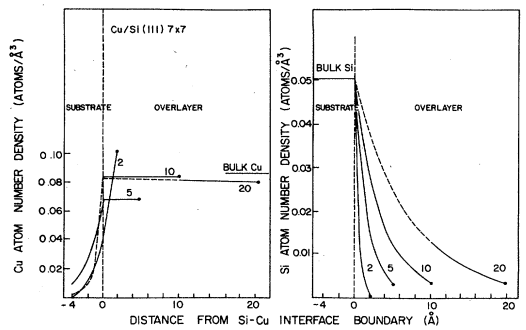

FIG. 10. Calculated Cu and Si atom number densities vs distance from the interface boundary. A dashed line signifies an extrapolation, since our maximum depth sensitivity is 3Λ (10 to 11 Å).

V. DISCUSSION

A. Comparison with other techniques

Interdiffusion at metal-semiconductor interfaces has been qualitatively studied recently by both angle-resolved and angle-integrated photoemission.[1,3–5,24,25] While outdiffusion of Si is relatively easy to observe by constructing attenuation curves similar to those in Fig. 3, diffusion of the metal into the substrate has been observed by comparing the rate of growth of the metal photoemission intensity with coverage to that expected for a sharp interface[24] and by performing marker experiments.[25] In the latter, a thin layer of an inert metal is deposited onto the substrate prior to evaporation of the metal of interest. Assuming the marker layer does not interfere with interdiffusion, the behavior of the substrate to marker intensity ratio with coverage indicates qualitatively whether or not indiffusion of the metal is occurring. The advantages of the method described here is that no marker layer (which may indeed perturb the interdiffusion process[26]) is needed and the quantitative extent of indiffusion can be obtained.

Other quantitative methods involving polar angle-resolved x-ray photoemission have been proposed recently. Specifically, Pijolet and Hollinger have attempted to extract density information directly from the polar profiles via a simplex method which minimizes the difference between theoretical and experimental intensity ratios.[27] However, this approach has proved to possess some serious difficulties. First, the extracted concentrations are extremely sensitive to the details of the polar profile. Intensity ratio changes on the order of 0.001% make substantial changes in the extracted concentrations. In order to

remedy the situation, they found that it was necessary to introduce two physically reasonable constraints on the concentrations. These consisted of (1) bracketing the concentration of each specie between zero and the bulk concentration for the pure material and (2) assuming a particular shape or trend in the density profile. Clearly, once such constraints are introduced, the method becomes quite analogous to what we present here. However, this "direct-extraction" method requires a number of involved numerical techniques which necessitate considerable computer time on a large mainframe computer. The method we introduce is relatively simple and can be run on any of the powerful microcomputers currently available.

B. The chemical nature of the interface region

The substantial line-shape changes in the Si($L_{2,3}VV$) peak clearly demonstrate that, upon interdiffusion, a strong electronic interaction occurs between Si and Cu. As the normal sp^3 hybrid bonds are broken in the Si lattice and outdiffusion occurs, the valence states are modified and new channels for Auger deexcitation are opened, thus modifying the Si($L_{2,3}VV$) spectrum.[22] Although the details of chemical environment are very difficult to extract from Auger line-shape analysis, the results presented here enable us to comment on the stoichiometry of the intermixed phase. Above a coverage of 2 Å, the Cu density in the overlayer is constant. However, the Si density drops very rapidly from interface to surface for all coverages. These results suggest that a copper silicide of fixed stoichiometry does not form in the intermixed region, as proposed earlier.[4] Rather, a Cu lattice which is rich in Si only near the interface appears to be a better description (see Fig. 8). This conclusion is consistent with valence-band photoemission results which show a dominant Cu-derived $3d$ feature that shifts from 3.5 eV below the Fermi level at submonolayer coverages to $\sim$2.8 eV at 45 monolayers, indicative of a transition from isolated Cu atoms to a pure Cu metallic phase.[3] If Cu diffuses into the substrate with a characteristic penetration depth of 1—2 Å as suggested by the use of Eqs. (10a) and (10b), it probably occupies defect and interstitial sites. This description of the interface is consistent with the bulk Cu-Si phase diagram which shows $\sim$2% solubility of Si in Cu at room temperature, and no compound formation at room temperature and Si percent by weight less than $\sim$8%.[28,29] The lack of solubility of Cu in Si, however, indicates that the slight indiffusion of Cu suggested here is the result of microscopic localized phenomena.

Although similar agreement between interface interdiffusion results and bulk phase information has been noted by Brillson *et al.*[25] for Al/Si(111)-7×7, agreement for Au/Si(111)-7×7 is lacking. The former is a weakly interacting chemisorption system, consistent with phase data. The latter, however, strongly interacts with considerable intermixing at room temperature, despite the inertness predicted by the phase diagram. Thus, it appears that bulk thermodynamic data are not of universal utility in predicting interface phenomena for noble metals adsorbed on Si single crystals.

VI. CONCLUSIONS

Angle-resolved Auger electron emission has been shown to be a powerful technique for the study of interdiffusion at a metal-semiconductor interface. Detailed, quantitative information on the composition of the interfacial region can be extracted from the polar-angle intensity profiles by means of a relatively simple theoretical model. By starting with physically reasonable density functions, a unique solution to the problem can be found by minimizing the difference between theory and experiment.

For the Cu/Si(111)-7×7 interface, a Si density function which decreases exponentially from the bulk Si value at the interface boundary to the surface is clearly the best description of the Si atomic distribution. For Cu, the best agreement between theory and experiment results from a density function which is constant in the overlayer and either terminates discontinuously or decreases exponentially into the substrate. Both functions generate good agreement with experimental polar profiles and with each other because the extent of Cu indiffusion is predicted by the latter to be very slight, i.e., after optimization, the two functions are quite similar. For both Si and Cu, the quality of the fit is sensitive to both the choice of density function and the choice of parameter(s). The primary source of uncertainty in this study is the diffraction modulation which is present at all coverages. The neglect of single-crystal effects in the theoretical model make it necessary to average over diffraction maxima and minima in fitting theory to experiment. This difficulty will not be present when other metal-semiconductor systems lacking long-range order are investigated in the future.

ACKNOWLEDGMENTS

This work was supported by a Northwest Area Foundation grant of Reseach Corporation for some of us (S.A.C., T.R.G., and G.A.H.) and the Army Research Office, Contract Nos. ARO-DAAG-29-83-K-0061 and ARO-DAAG29-84-K-0169 for one of us (J.H.W.). Stimulating discussions with Dr. M. Grioni are gratefully acknowledged.

[1]For an extensive review of metal/semiconductor interfaces, see L. J. Brillson, Surf. Sci. Rep. **2**, 123 (1982).
[2]M. Grioni, J. Joyce, S. A. Chambers, D. G. O'Neill, M. del Giudice, and J. H. Weaver, Phys. Rev. Lett. **53**, 2331 (1984).
[3]F. Ringeisen, J. Derrien, E. Daugy, J. M. Layet, P. Mathiez, and F. Salvan, J. Vac. Sci. Technol. **B1**, 546 (1983).
[4]G. Rossi, T. Kendelewicz, I. Lindau, and W. E. Spicer, J. Vac. Sci. Technol. **A1**, 987 (1983).
[5]*Thin Films—Interdiffusion and Reactions,* edited by J. M. Poate, K. N. Tu, and J. W. Mayer (Wiley, New York, 1978).
[6]J. W. Coburn, J. Vac. Sci. Technol. **13**, 1037 (1976).
[7]T. Ishitani and R. Shimizu, Appl. Phys. **6**, 241 (1975).
[8]H. H. Andersen, Appl. Phys. **18**, 131 (1979).
[9]P. S. Ho and J. E. Lewis, Surf. Sci. **55**, 335 (1976).

[10]J. M. Guglielmacci and M. Gillet, Surf. Sci. **94**, 424 (1980).
[11]N. J. Chou and M. W. Shafer, Surf. Sci. **92**, 601 (1980).
[12]C. S. Fadley and S.A.L. Bergstrom, Phys. Lett. **35A**, 375 (1971).
[13]C. S. Fadley, in *Electron Spectroscopy: Theory, Techniques, and Applications,* edited by C. R. Brundle and A. D. Baker (Academic, London, 1978), Vol. 2, Chap. 1.
[14]N. G. Stoffel, M. Turowski, and G. Margaritondo, Phys. Rev. B **30**, 3294 (1984).
[15]C. S. Fadley, in *Progress in Solid State Chemistry,* edited by G. A. Somorjai and J. O. McCaldin (Pergamon, New York, 1976), Vol. 11, pp. 275-284.
[16]S. Kono, S. M. Goldberg, N. F. T. Hall, and C. S. Fadley, Phys. Rev. B **22**, 6085 (1980).
[17]J. E. Rowe and H. Ibach, Phys. Rev. Lett. **32**, 421 (1974).
[18]D. W. Marquardt, J. Soc. Ind. Appl. Math. **11**, 431 (1963).
[19]S. A. Chambers and L. W. Swanson, Surf. Sci. **131**, 385 (1983).
[20]J. M. McDavid and S. C. Fain, Surf. Sci. **52**, 670 (1975).
[21]R. Matz, R. J. Purtell, Y. Yokota, G. W. Rubloff, and P. S. Ho, J. Vac. Sci. Technol. **A2**, 253 (1984).
[22]P. S. Ho, G. W. Rubloff, J. E. Lewis, V. L. Moruzzi, and A. R. Williams, Phys. Rev. B **22**, 4784 (1980).
[23]I. Lindau and W. E. Spicer, J. Electron Spectrosc. Relat. Phenom. **3**, 409 (1974).
[24]L. Braicovich, C. M. Garner, P. R. Skeath, C. Y. Su, P. W. Chye, I. Lindau, and W. E. Spicer, Phys. Rev. B **20**, 5131 (1979).
[25]L. J. Brillson, A. D. Katnani, M. Kelly, and G. Margaritondo, J. Vac. Sci. Technol. **A2**, 551 (1984).
[26]A. Franciosi, J. H. Weaver, and D. G. O'Neill, Phys. Rev. B **28**, 4889 (1983).
[27]M. Pijolat and G. Hollinger, Surf. Sci. **105**, 114 (1981).
[28]M. Hansen, *Constitution of Binary Alloys,* 2nd ed. (McGraw-Hill, New York, 1958).
[29]R. P. Elliot, *Constitution of Binary Alloys, First Supplement* (McGraw-Hill, New York, 1965).